Proceedings of
2001 ASME International Mechanical Engineering Congress and Exposition
November 11-16, 2001, New York, NY

IMECE2001/HTD-24411

APPLICATION OF A TWO-COLOR LASER INDUCED FLUORESCENCE (LIF) TECHNIQUE FOR TEMPERATURE MAPPING

H. J. Kim and K. D. Kihm*
Department of Mechanical Engineering
Texas A&M University
College Station, Texas, 77843-3123
*E-mail : ken-kihm@tamu.edu, Homepage : [http://go.to/microlab]
Tel. (979) 845-2143, Fax (979) 862-2418

ABSTRACT

Two-color laser induced fluorescence (LIF) technique has been developed and examined to use for full-field temperature mapping of a micro-scale field-of-view in water. The technique uses two fluorescence dyes with different emission characteristics – one is the temperature sensitive dye (Rhodamine-B) and the other is the temperature insensitive dye (Rhodamine-110). The ratio of the two fluorescence emission intensities, therefore, provides a formidable correlation with temperature that does not depend on the laser illumination intensity variation and is free from the possible bias occurring from background noise. In considering the technique for applications to micro-scale field-of-view, the first question that may be asked will be if the technique ensures acceptable accuracy in temperature readings with sufficiently small spatial resolution. In order to explore answers to this question, an extensive calibration for the intensity ratio versus temperature has been performed using a constant-temperature bath and the calibration results have been statistically analyzed to estimate measurement uncertainties. The developed technique measures thermally stratified fields with known temperature distributions that are established inside 10-mm and 1-mm path cuvettes to ensure measurement accuracy and spatial resolution for potential microscale applications.

1. INTRODUCTION

Among the available means of temperature measurement probes, there is no question on the extensiveness and rigorousness of thermocouple (TC) probes for a wide range of heat transfer applications. A carefully calibrated TC probe is capable of measuring temperature with better than ± 0.1 K precision [1]. Two primary limitations of TC probes, however, are their relatively large spatial resolution, on the order of a few hundred microns at the smallest, and their physical intrusiveness in the flow. These limitations diminish the possibility of using TC probes for microscale heat transfer applications. In addition, their point measurement nature makes full-field temperature mapping very cumbersome as a large number of probes must be placed and monitored simultaneously.

Thermo-chromic liquid crystal (TLC) probes have been widely used for temperature measurement as a nonintrusive and full-field mapping technique [2,3]. The TLC technique is based on the temperature dependence of their optical properties in a predictable and repeatable manner. When TLC is illuminated, TLC selectively reflects light at a visible wave length characterized by the local temperature. This relationship of color to temperature has allowed researchers to quantitatively map temperature distribution. More recently, Richards et al. [4] showed measurements of temperature distributions in a convectively cooled droplet. In their experiment, microencapsulated beads of TLC, suspended in the water droplet, enabled the visualization of the transient temperature fields within the droplet. Pehl et al. [5] examined the dependence of the thermochromic nature of TLC probes on medium pressure.

A major shortcoming in using TLC is that one has to calibrate each point of test field to compensate for the influence of the illuminating light variation [6]. Since the color change of the TLC may also depend on its location in the test field, the temperature calibration has to be tediously repeated at each different test section. The color bias occurring from the wall reflection and scattering is another obstacle in applying the TLC technique to full-field mapping. Another major drawback of the TLC technique for considering microscale field-of-view measurements is the relatively larger sizes of microencapsulated TLC beads, typically on the order of 10 μm or larger.

The Laser Induced Fluorescence (LIF) technique [7] uses fluorescence dye molecules of approximately 10-nm size as seeding particles and seems more appropriate for microscale applications. Nakajima et al. [8] and Satoh and Kasagi [9] showed LIF as a feasible temperature mapping technique using temperature sensitive fluorescence dyes. Coolen et al. [10] applied the LIF technique to measure the 12-cm by 5-cm planar test field of a buoyancy-driven temperature field using Nd-Yag laser as the fluorescence pumping source. The fluorescence intensity is proportional to the illuminating light intensity, dye concentration and optical constant of the dye called quantum efficiency [11]. Therefore, if the illumination light is perfectly uniform and the dye concentration remains constant, the fluorescence intensity may be considered, in principle, to depend only on temperature. However, in practice, it is very difficult to ensure a homogeneous incident light intensity distribution, if not impossible, and the imperfection of recording means can hardly guarantee

persistent intensity levels even under uniform lighting and constant dye concentration.

To overcome this problem, Sakakibara and Adrian [12,13] recently proposed an innovative two-color LIF technique where they used a second temperature-insensitive fluorescence dye as a reference to compensate for the variation of incident light and the spatial imaging nonuniformity. Their results showed a measurement accuracy of ±1.5 K over a 25 K temperature range. They applied this technique to measure a three-dimensional thermal convection field above a heated horizontal surface of 40-mm square in dimension.

The present study adopts a similar two-color LIF technique to examine the feasibility of using the technique for microscale temperature field-mapping. Rhodamine-B is used as a temperature-sensitive probe dye and rhodamine-110 is used as a non-temperature-sensitive reference dye. The ratio of the fluorescence emissions from the two dyes is taken as a measure of temperature reading. In section 2, the basic principle of fluorescence is briefly discussed. A brief discussion of the spectral characteristics of two-color fluorescence is presented in Section 3. Section 4 presents the necessary calibration process and its statistical interpretation in terms of temperature uncertainties and spatial resolution. In section 5, application of the calibrated two-color LIF technique is presented for measurement of stratified temperature fields established in 1-cm and 1-mm scale cuvette channels. Section 6 discusses a few fundamental conclusions.

2. PRINCIPLES OF FLUORESCENCE AND RATIOMETRIC LIF TECHNIQUES

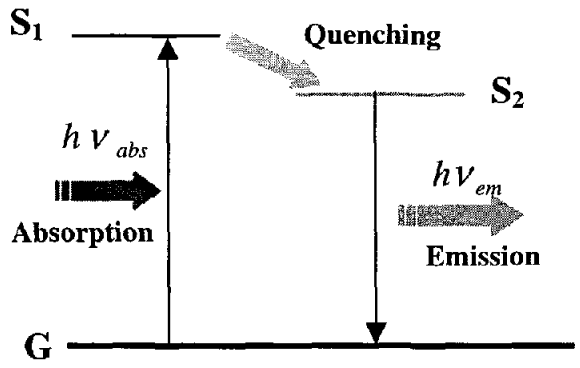

Fig. 1 The creation of an excited electronic single state by optical absorption and subsequent emission of fluorescence

Fluorescence is the property of an atom or a molecule that is excited by incident light at a particular wavelength to a stimulated absorption state at a higher quantum energy level, and after a very short interval, termed the fluorescence lifetime, re-emits light at longer wavelengths (Fig. 1). Fluorescence intensity at a specified point is expressed as [14]:

$$F = I_0 \varepsilon [c] Q \qquad (1)$$

where F is the measured fluorescence intensity for a fluorescent dye with molar absorptivity of ε at a point in the incident light with intensity I_0, with the fluorescence dye concentration $[c]$, and the quantum efficiency Q.

Fluorescent molecules that absorb energy move from ground state (G) to the exited state (S_1), as schematically illustrated in Fig. 1. The quenching effect makes relaxation or non-radiative emission to the lower excited state (S_2), decreasing the quantum efficiency Q to less than unity. As the temperature increases, the quenching effect increases and the quantum efficiency decreases. The temperature dependence of quantum efficiency is usually small in most fluorescent molecules. However, for some fluorescence dyes such as Rhodamine-B, the temperature dependence of quantum efficiency is noticeably high, about 2%/K. As mentioned previously, fluorescent light intensity is proportional to the incident light intensity. Incident light is likely to be inhomogeneous, spatially as well as temporally, because of the laser beam or sheet divergence, scattering by small particles in the beam path, and time-dependent lasing efficiency [13]. In order to compensate the measurement bias caused by the incident light variation, Rhodamine-110 is used for the reference dye whose photo-thermal sensitivity is known to be less than 0.05%/K.

For the mixture of Rhodamine-B and Rhodamine-110, the intensity ratio of the two fluorescence emissions can be directly given from Eq. (1) as:

$$\frac{F_{rhb}}{F_{rh110}} = \frac{I_{0\,rhb}\varepsilon_{rhb}[c]_{rhb}Q_{rhb}}{I_{0\,rh110}\varepsilon_{rh110}[c]_{rh110}Q_{rh110}} \qquad (2)$$

where molar absorptivity ε is nearly independent of temperature [11], and the ratio of the absorption spectral intensity, I_{0rhb}/I_{0rh110}, is invariant when a single illumination source is used for both dyes. In addition, if the concentration ratio, $[c]_{rhb}/[c]_{rh110}$, remains unchanged, the fluorescence intensity ratio, F_{rhb}/F_{rh110}, is solely dependent on the quantum efficiency ratio of the two dyes, Q_{rhb}/Q_{rh110}. Since the ratio of the quantum efficiency depends on temperature, the resulting intensity ratio of Eq. (2) can now be considered solely dependent on temperature.

3. SPECTRAL CHARACTERISTICS OF TWO-COLOR FLUORESCENCE

Figure 2 shows the semi-quantitative absorption and emission spectra of Rhodamine-B and Rhodamine-110. The wavelength of maximum absorption and emission for Rhodamine-110 (Molecular Probes) is at 496-nm and 520-nm, respectively. Rhodamine-B (J. T. Baker, Inc.) has an absorption band peaked at 554-nm and an emission band peaked at 575-nm. These four bandwidths partially overlap each other. To minimize signal errors due to the cross-talk, the fluorescence detection band for each dye must be segregated from the other emission and absorption bandwidths, to the extent possible. For the Rhodamine-B detection bands, selection is made for the long pass filter (Edmund Industrial Optics) that transmits wavelengths only longer than 560-nm. This filter has a mere 0.001% transmission of shorter wavelengths than 560-nm. Since Rhodamine-110 emission band is placed between the Rh-110 absorption band and Rh-B absorption band, a narrow band-pass filter (505-nm ~ 515-nm) is selected to effectively separate the Rh-110 emissions. The spectral band of an argon-ion laser, peaked at 488-nm (blue), is used to excite both dyes.

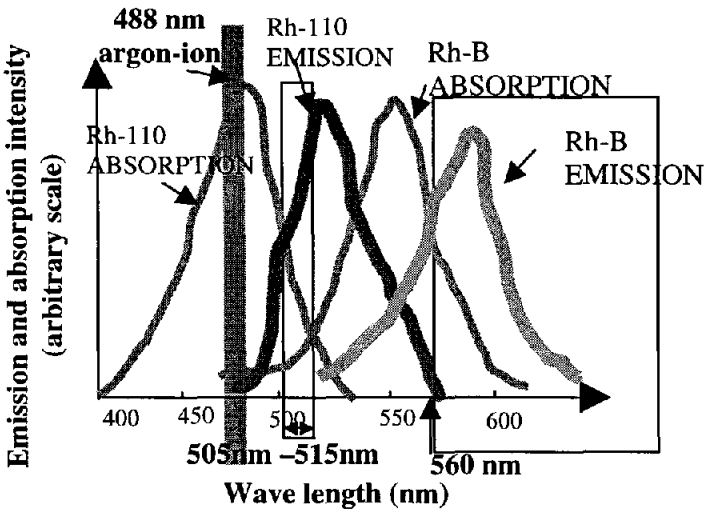

Fig. 2 Absorption and fluorescence spectra of Rhodmine-110 and Rhodamine-B

4. CALIBRATION PROCESS

The correlation between fluorescence intensity and temperature is necessary to use a LIF technique for temperature measurement. To obtain a correlation between the measured fluorescence intensity and the water temperature, an elaborate calibration system is devised using a constant thermobath as schematically illustrated in Fig. 3. The thermobath circulates constant-temperature water through a 15-cm cubic chamber which is made of 0.6-cm thick plexiglass walls covered with ample insulation material to minimize the ambient thermal effect. A 3.5-cm square glass window has been installed on the front wall for optical access. The test cuvette (Cole Parmer) contains a 6-mg/liter concentration of Rh-B and 1-mg/liter concentration of Rh-110, and the cuvette is placed in the midst of the cubic chamber. The water temperature surrounding the cuvette is monitored using a thermocouple probe placed in the chamber.

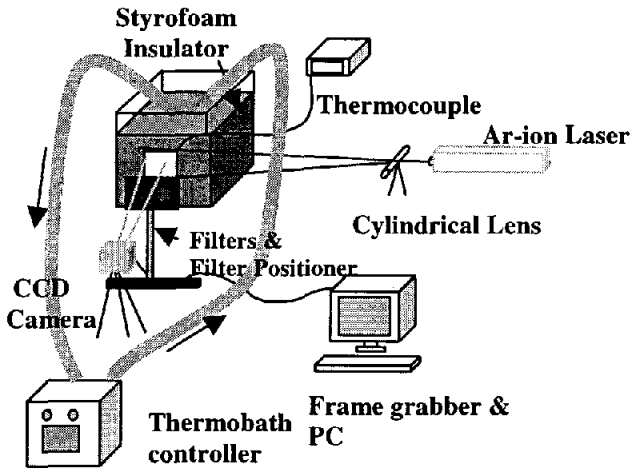

Fig. 3 Schematic layout of the calibration setup for two-color LIF technique

A Sony XC-75 CCD camera records fluorescence images from Rh-B and Rh-110 by alternating the two filters and an approximately 1.5-mm by 1.0-mm field-of-view is used for calibration, corresponding to 320 x 240 pixel dimensions. A thin laser sheet is constructed from a 50-mW argon-ion laser using a combination of one concave lens and one spherical lens. Captured images from the CCD camera are digitized for successive gray-level analysis. The key to success in calibration is to ensure the repeatability of the calibration curves and the persistency in dye concentrations for each calibration process. Due to chemical and photochemical decomposition, the intensity of fluorescence dye may degrade during excitation and emission transitions [13]. Therefore, a fresh mixture of fluorescence dyes has to be used for each run of the calibration experiment.

The left column of Fig. 4 shows a series of fluorescence images (1.5-mm by 1.0-mm field-of-view) taken for Rh-B for four different bath temperatures, the center column shows corresponding images for Rh-110, and the right column presents the ratio of the two images, the former to the latter. The Rh-B images clearly show the temperature dependence of the intensity that decreases with increasing temperatures whereas Rh-110 images are nearly invariant with temperature increases. The background intensity variations, in sub-millimeter or micron-scale, shown for the individual fluorescence images reflect the light ray nonuniformity occurring from the nonuniform laser beam characteristics, imperfect lens curvature, particularly of the negative concave lens surface, varying refractive index due to thermal variation, and suspending impurities in the circulating water. When the Rh-B images are normalized by the corresponding Rh-110 images, the background variations are cancelled out and the resulting ratio images are highly homogeneous showing a monotonic decrease with increasing temperature.

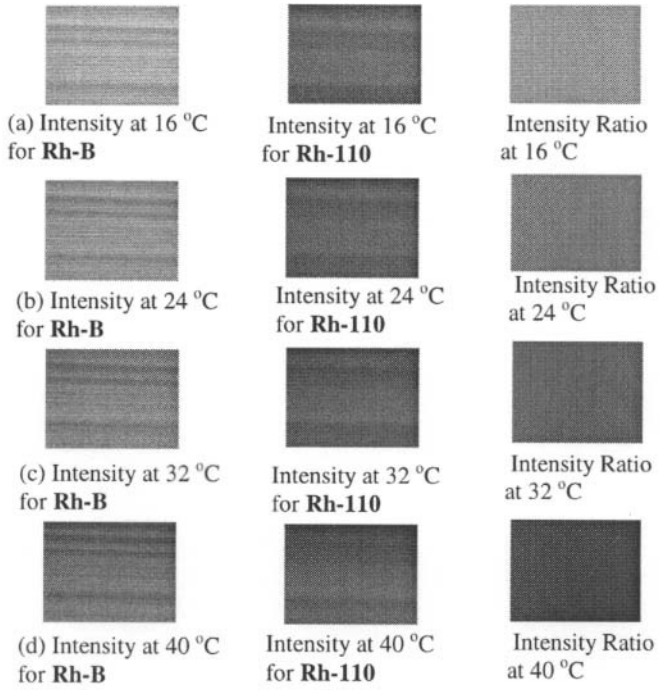

Fig. 4 Temperature dependence of fluorescence images of Rh-B (left column), Rh-110 (center column), and their ratiometric images (right column)

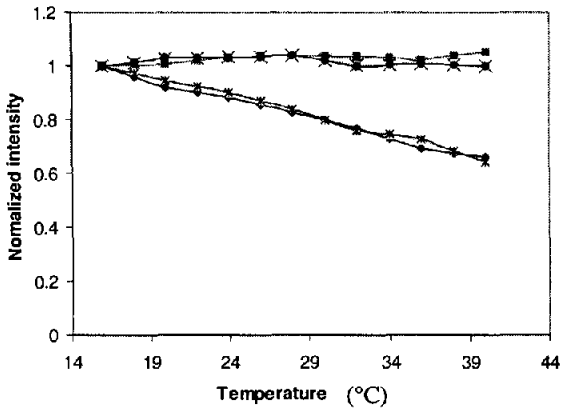

(a) Temperature dependence of fluorescence image intensities for Rh-B and Rh-110

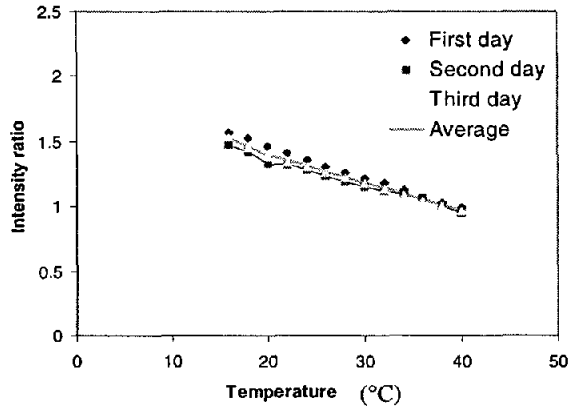

(b) Temperature dependence of the ratiometric image intensities

Fig. 5 Temperature dependence of fluorescence images

In order to ensure the repeatability, the calibration was repeated on three different test days for the same temperature range from $16\,^{\circ}C$ to $40\,^{\circ}C$. Figure 5-a shows measured intensity variations for the two dyes that are individually normalized by the intensity taken at $16\,^{\circ}C$. Each symbol represents a pixel-averaged intensity for the entire 1.5-mm x 1.0-mm field-of-view (320 by 240 pixels). The fluorescence intensity of Rh-B decreases with increasing temperature while the fluorescence intensity of Rh-110 remains nearly constant. The day-to-day variations are smaller than 5%, which may be attributed to the several aforementioned reasons. Figure 5-b presents the same calibration data in terms of the intensity ratio of Rh-B over Rh-110. The average of the three sets of calibration data, shown by the solid curve, can now be used as a resulting calibration curve for temperature measurement. The day-to-day variations of the intensity ratio show a decrease with increasing temperatures, however the normalized intensity variation, with respect to the average value, i.e., the AC-component normalized by the DC-offset, remains nearly constant.

An important thing to note is that the variations shown in Figs. 5-a and b are based on the smallest spatial resolution of a single pixel, that is equivalent to a spatial resolution of about 4.7 μm by 4.2 μm. To examine the effect of spatial resolution on the intensity variations, statistical analysis of the calibration data has been conducted as the interrogation cell size is increased from a single pixel to the whole field-of-view.

Table 1 Spatial-resolution dependency of the calibration uncertainties of two-color LIF technique

Interrogation window Dimension (pixels)	Spatial Resolution (μm)	Intensity Ratio Deviation	Temperature Deviation (^{o}C)
1 by 1	4.7 × 4.2	±0.143	±5.635
10 by 10	47 × 42	±0.056	±2.964
32 by 24	150 × 100	±0.043	±1.967
64 by 48	300 × 200	±0.033	±1.496
320 by 240	1500 × 1000	±0.000	±0.000

Table 1 summarizes the results where the standard deviation is calculated for each calibration temperature with 95% confidence interval for a given interrogation cell size and listed deviations are the average values for the tested temperature range from 16 to $40\,^{\circ}C$. The intensity ratio deviations are presented in the third column and the corresponding temperature deviations are shown in the fourth column. As the interrogating window dimension increases, the variation of intensity ratio decreases and diminishes ultimately to zero when the whole field-of-view is considered as a single interrogation window.

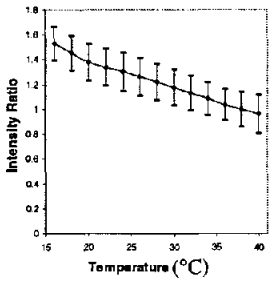

(a) Interrogation window dimension of 1 by 1 pixel (4.7μm × 4.2μm)

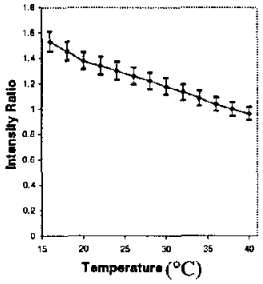

(b) Interrogation window dimension of 10 by 10 pixels (47μm × 42μm)

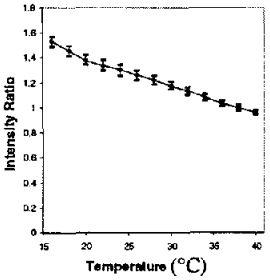

(c) Interrogation window dimension of 64 by 48 pixels (300μm × 200μm)

Fig. 6 Deviation of intensity Ratio vs. Temperature

Figures 6-a, b and c show the average and standard variation of the intensity ratio as functions of temperature for the selected three different interrogating window dimensions of 1 by 1 pixels (4.7 μm x 4.2 μm), 10 by 10 pixels (47 μm x 42 μm), and 64 by 48 pixels (300 μm x 200 μm), respectively. Figures 7-a, b and c present the measured temperature variations versus the imposed temperature by converting the intensity ratio, shown in Figs. 6-a, b and c, using the calibration curve presented in Fig. 5. The corresponding pixel-to-pixel temperature variation (Table 1) is estimated as $\pm$ 5.64 K for 1 by 1 pixel, approximately $\pm$ 3.0 $^{\circ}$ K for 10 by 10 pixels, $\pm$ 2.0 K for 32 by 24 pixels, and $\pm$ 1.5 K for 64 by 48 pixels with 300 μm x 200 μm spatial resolution. While the standard variations of intensity ratios, for a given temperature, persistently increase with decreasing window dimensions, note that the average intensity ratio remains constant for a given temperature regardless of the spatial resolution.

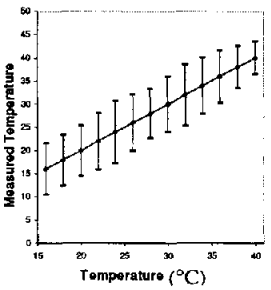

(a) Interrogation window dimension of 1 by 1 pixel (4.7μm × 4.2μm)

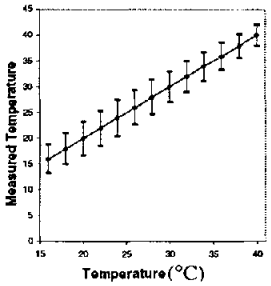

(b) Interrogation window dimension of 10 by 10 pixels (47μm × 42μm)

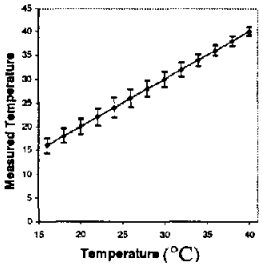

(c) Interrogation window dimension of 64 by 48 pixels (300μm × 200μm)

Fig. 7 Deviation of Measured Temperature from Specified Temperature

5. TEMPERATURE MEASUREMENTS FOR THERMALLY STRATIFIED FIELDS

For a thermally stratified region in a parallel channel with the top surface heated and the bottom cooled, in the absence of heat generation, a linear temperature distribution is expected for the fluid between the two surfaces. The linear temperature profile will remain stationary if the boundary temperature conditions are persistent and heat loss through side surfaces is eliminated. Using the developed and calibrated two-color LIF technique, temperature profiles have been mapped for thermally stratified regions under different temperature differentials. Measurement accuracy and spatial resolution have been examined for both the 10-mm and 1-mm path parallel channels. The same cuvette used for the calibration (10-mm x 10-mm x 40-mm) serves for the 10-mm parallel channel and a 1-mm height, 10-mm width, and 40-mm length cuvette (Nova Biotech) is used for the 1-mm channel configuration.

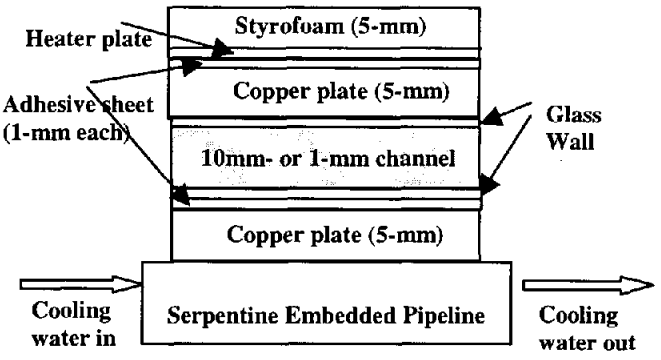

Fig. 8 Experimental layout for the test parallel channel

Figure 8 illustrates the test channel to establish a thermally stratified flow region. A flexible heater strip of about 100-μm thickness (Omega Inc.) is placed on the top surface of the cuvette which is made of 1-mm thick glass plate. To ensure more homogeneous thermal contact, a 5-mm thick copper block is inserted between the heater strip and the cuvette glass surface and bonded by thermal-conducting epoxy. A thermocouple probe is embedded to 0.5-mm deep inside the copper block from the contacting surface with the glass plate. The temperature reading is fed as a feedback signal to the heater control unit to maintain a constant heater surface temperature constant. For cooling of the bottom surface, a copper block is again inserted to ensure uniform thermal contact and cooling water is circulated through a serpentine pipeline attached to the bottom of the copper block. It typically takes up to 30 minutes for both sides to reach the required temperature conditions. The test channels contain an identical mixture of the two dyes as was used for the calibration (6-mg/liter for Rh-B and 1-mg/liter for Rh-110).

Figure 9 shows false-colored images of measured distributions of the intensity ratio for the 10-mm thermally stratified region of four different temperature differentials, 17 $^{\circ} C$, 14 $^{\circ} C$, 6 $^{\circ} C$, and 3 $^{\circ} C$. Only the central 8.3-mm region of the 40-mm long test cuvette is shown in Fig. 9 and the horizontally line-averaged temperature values are presented as functions of the channel height in Fig. 10. The intensity ratio images (Fig. 9) qualitatively and quantitatively show the thermally stratified characteristics inside the 10-mm channel. Figure 10 shows that the maximum deviations of measured data from the ideal prediction of a linear profile are up to 2 $^{\circ} C$ at the largest. The deviation amount grows with decreasing temperature differential as its relatively weakly defined stratified layers may attribute to the larger uncertainties in thermal stratification. The liquid surface temperature is assumed identical as the TC-measured temperature reading at 0.5-mm below the copper surface, which is separated by the 1-mm thick glass wall from the channel water. This may have attributed to the biasing of the field temperature. The flow deviating from perfect stratification is also expected to occur because of the possible convection flow rendering inside the cuvette that is not perfectly adiabatic against the lab environment. The test uncertainty based on the imperfect test flow conditions, together with the inherent diagnostic uncertainties of the LIF technique (Table 1), has been combined in the data discrepancies shown in Fig. 10. Nevertheless, the LIF results, without any

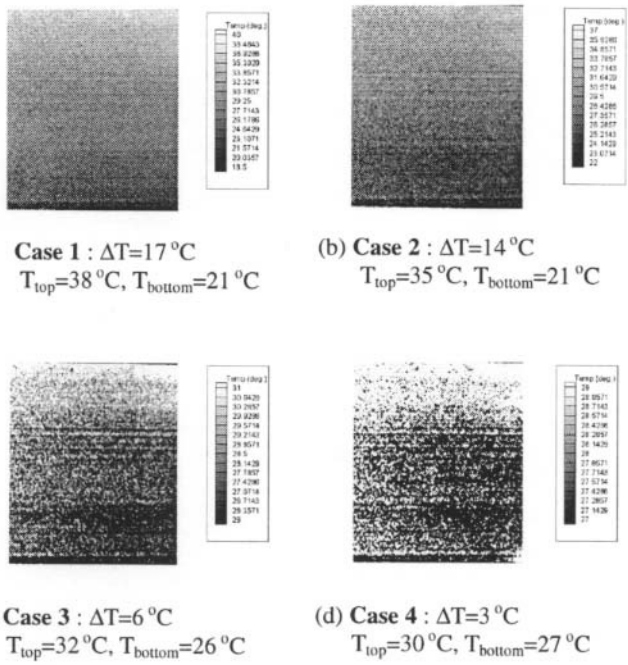

(a) **Case 1** : ΔT=17 °C
T_{top}=38 °C, T_{bottom}=21 °C

(b) **Case 2** : ΔT=14 °C
T_{top}=35 °C, T_{bottom}=21 °C

(c) **Case 3** : ΔT=6 °C
T_{top}=32 °C, T_{bottom}=26 °C

(d) **Case 4** : ΔT=3 °C
T_{top}=30 °C, T_{bottom}=27 °C

Fig. 9 Temperature field for 10mm channel

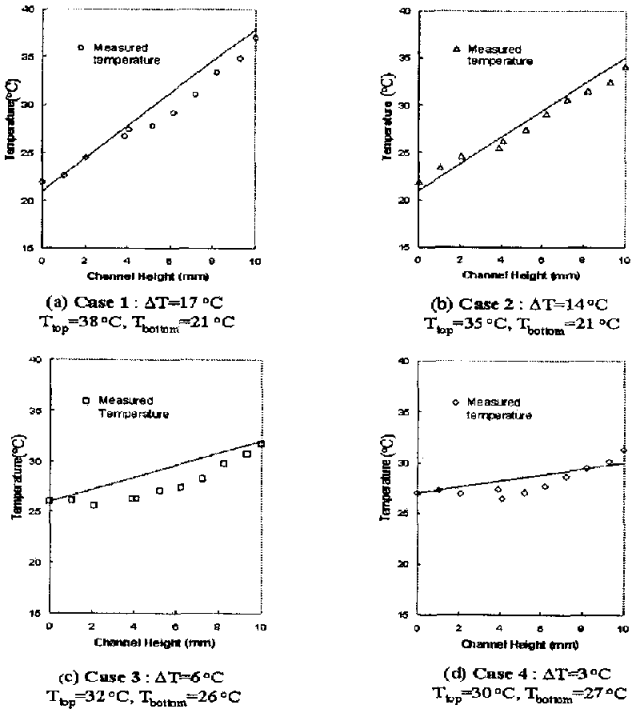

(a) **Case 1** : ΔT=17 °C
T_{top}=38 °C, T_{bottom}=21 °C

(b) **Case 2** : ΔT=14 °C
T_{top}=35 °C, T_{bottom}=21 °C

(c) **Case 3** : ΔT=6 °C
T_{top}=32 °C, T_{bottom}=26 °C

(d) **Case 4** : ΔT=3 °C
T_{top}=30 °C, T_{bottom}=27 °C

Fig. 10 Temperature profile for the 10-mm channel

parametric adjustment, imposed specification, or often-misleading normalization between experimental data and predictions, show fairly impressive agreement with the ideal solution of linear profiles for all the tested cases

For the case of the 1-mm channel, the central 750-μm regions of intensity ratio distributions are shown for four different temperature differentials ranging from 18 $^{\circ}C$ to 2 $^{\circ}C$ in Fig. 11. The spatially resolvable scale of Fig. 11 is clearly increased from that of the 10-mm channel (Fig. 9), and the spatial resolution for the present measurement system is conservatively estimated to be approximately 50 μm for the case of 1.0-mm field-of-view dimension. The false-colored images clearly show that the thermally stratified characteristics are distinctive for the relatively larger temperature differentials of 18 $^{\circ}C$ and 12 $^{\circ}C$ (Figs. 11-a and b), and the stratification characteristics are reduced for the smaller temperature differentials of 5 $^{\circ}C$ and 2 $^{\circ}C$ (Figs. 11-c and d).

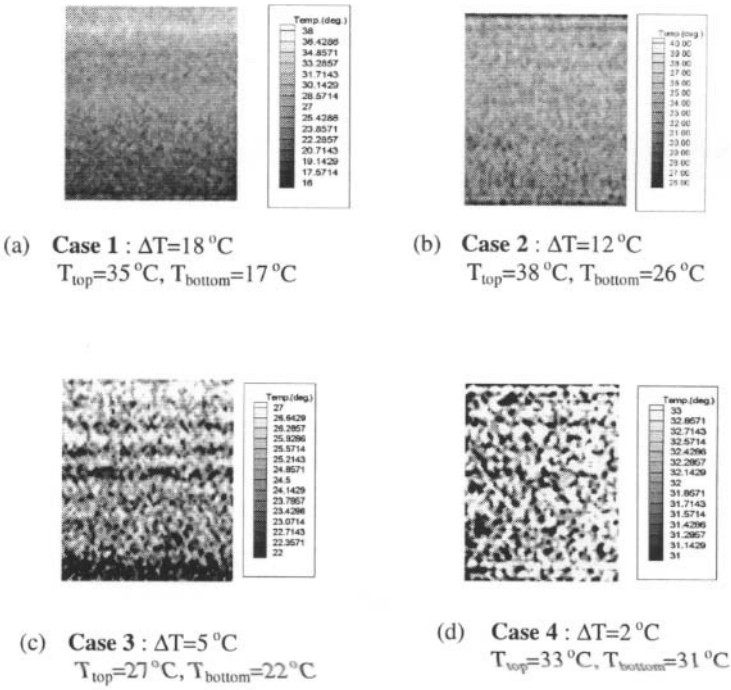

(a) **Case 1** : ΔT=18 °C
T_{top}=35 °C, T_{bottom}=17 °C

(b) **Case 2** : ΔT=12 °C
T_{top}=38 °C, T_{bottom}=26 °C

(c) **Case 3** : ΔT=5 °C
T_{top}=27 °C, T_{bottom}=22 °C

(d) **Case 4** : ΔT=2 °C
T_{top}=33 °C, T_{bottom}=31 °C

Fig. 11 Temperature field for 1mm channel

Figure 12 shows the line-averaged temperature values calculated from the pixel grey level distributions corresponding to Fig. 11. The deviations between the measured data and the ideal predictions are less than 1 $^{\circ}C$, which is two-times better than the accuracy observed for the 10-mm channel. This reduced discrepancy may be attributed to the more strongly defined thermal stratification for the 1-mm channel with larger

aspect ratio. The results show fairly good potential of the two-color LIF full-field temperature mapping technique for microscale thermal field applications with a spatial resolution on the order of 10 μm .

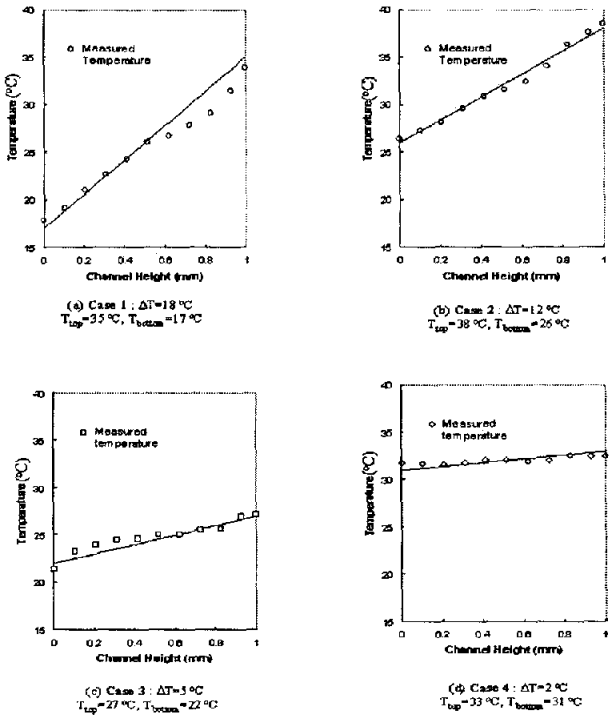

Fig. 12 Temperature profile for the 1-mm channel

6. CONCLUSION

Two-color Laser Induced Fluorescence (LIF) technique has been developed and examined for its potential use for microscale temperature mapping. Detection of the fluorescence intensity ratio of the temperature-sensitive Rh-B to the temperature-insensitive Rh-110 enables temperature measurements that are free from the background noise occurring primarily from the nonuniformity of incident laser sheet. The measurements for thermally stratified regions inside 10-mm and 1-mm channels show fairly good accuracy compared with their known computational solutions. The estimated spatial resolution is on the order of 10 μm and the measurement accuracy is found to be better than 1.0 °C for the 1-mm channel, and up to 2.0 °C for the 10-mm channel. Results show that the two-color LIF technique has good potential for use in measuring micro-scale temperature fields. The temperature uncertainty for a typical spatial resolution of 300μm by 200μm is estimated to be ±1.45 °C with a 95% confidence interval.

REFERENCES

[1] Eckert, E. R. G. and Goldstein, R. J., 1970, Measurements in Heat Transfer, McGraw-Hill, New York.

[2] Dabiri, D. and Gharib, M., 1990, "Digital particle image thermometry and its application to a heated vortex ring," Fluid Measurement and Instrumentation Forum. ASME FED. 95: 27-34.

[3] Dabiri, D. and Gharib, M., 1991, "Digital particle image thermometry: The method and implementation," Experiments in Fluids, **11**, pp. 77-86.

[4] Richards, C. D. and Richards, R. F., 1998, "Transient temperature measurements in a convectively cooled droplet," Experiments in Fluids, **25**, pp. 392-400.

[5] Pehl, M., Werner, F., and Delgado, A., 2000, "First visualization of temperature fields in liquids at high pressure using thermochromic liquid crystals," Experiments in Fluids, **29**, pp. 302-304.

[6] Sabatino, D. R., Praisner, T. J., Smith, C. R., 2000, "A high-accuracy calibration technique for thermochromic liquid crystal temperature measurements," Experiment in Fluids, **28,** pp. 497-505.

[7] Chu, S. S. and Grigoropoulos, C. P., 2000, "Determination of kinetic energy distribution in a Laser-Ablated titanium plume by emission and Laser-Induced Fluorescence Spectroscopy," Journal of Heat Transfer, Nov. 2000, Vol. 122, pp. 771-775.

[8] Nakajima, T., Utsunomiya, M., Ikeda, Y. and Matsumoto, R., 1990, "Simultaneous measurement of velocity and temperature of water using LDV and fluorescence technique," 5th Int. Symp. on Application of Laser Tech. To Fluid Mech., Lisbon, 2.6.1-2.6.6.

[9] Sato, K. and Kasai, N., 1997, "Combined velocity and scalar field measurement with the simultaneous use of scanning PIV and LIF," The 10th Int. Symposium on Transport Phenomena in Thermal Science and Process Engineering (ISTP10), to be published.

[10] Coolen, M. C. J., Kieft, R. N., Rindt, C. C. M., and van Steenhoven, A. A., 1999, "Application of 2-D LIF temperature measurements in water using a Nd-Yag laser," Experiments in Fluids, **27,** pp. 420-426.

[11] Andrews, D. L., 1986, Lasers in Chemistry, Springer-Verlag, Berlin.

[12] Sakakibara, J. and Adrian, R. J., 1997, "Measurement of whole field temperature using two-color LIF," J. Visualization Soc., Japan 17:333-336.

[13] Sakakibara, J. and Adrian, R. J., 1999, "Whole field measurement of temperature in water using two-color laser induced fluorescence," Experiments in Fluids, **26,** pp. 7-15.

[14] Herman, B., 1998, "Fluorescence Microscopy," Second Edition, Springer.

[15] Salor. J. R., 1995, "Photobleaching of disodium fluorescein in water," Experiments in Fluids, **18,** pp. 445-447.